New York, 1987), p. 214].
16. B. Baker, G. Coupland, N. Fedoroff, P. Starlinger, J. Schell, *EMBO J.* **6**, 1547 (1987).
17. E. M. Attfield and P. K. Evans, *J. Exp. Bot.* **42**, 51 (1991).
18. S. Satina, A. F. Blakeslee, A. G. Avery, *Am. J. Bot.* **27**, 895 (1940).
19. C. Broertjes and A. M. Van Harten, *Application of Mutation Breeding Methods in the Improvement of Vegetatively Propagated Crops* (Elsevier, Amsterdam, 1978).
20. H. Dermen, *Am. J. Bot.* **40**, 154 (1953).
21. R. N. Stewart and L. G. Burk, *ibid.* **57**, 1010 (1970).
22. E. W. Weiler, *Planta* **149**, 155 (1980).
23. J. Porath, F. Maisano, M. Belew, *FEBS Lett.* **185**, 306 (1985).
24. D. Rodbard, *Clin. Chem.* (*N.Y.*) **20**, 1255 (1974).
25. C. Koncz and J. Schell, *Mol. Gen. Genet.* **204**, 383 (1986).
26. J. Sambrook, E. F. Fritsch, T. Maniatis, *Molecular Cloning* (Cold Spring Harbor Laboratory, Cold Spring Harbor, NY, 1989).
27. The 4.7-kb Xba I bands are composed of the right part of the *Ac* transposable element plus the *ipt* coding and termination regions (see Fig. 1), and represent *Ac* donor sites. "Empty donor sites" (regions from which *Ac* has excised) are detected as bands of higher molecular weight in Xba I digests, and are reduced to bands of approximately 1.7 kb in Eco RI–Xba I double digests (large arrows). Bands indicated by small arrowheads are *Ac* donor sites, because they hybridize to *Ac*-specific probes, and they have a molecular weight higher than 4.7 kb most likely due to DNA methylation (*28*) of Xba I site (or sites) located at the 3′ end of the 35*S-Ac-ipt* construct.
28. M. A. Van Sluys, J. Tempe, N. Fedoroff, *EMBO J.* **6**, 3381 (1987).
29. R. F. Barker, K. B. Idler, D. V. Thompson, J. D. Kemp, *Plant Mol. Biol.* **2**, 335 (1983).
30. Leaves from 35*S-Ac-ipt* transgenic plants that present one or two small bulges are considered slightly altered, whereas those with either few big bulges or many small ones are said to be severely altered. The term "teratoma-like" refers to adventitious buds that develop abnormally giving tumorous masses.
31. The RNA blot was hybridized first to an *ipt*-specific probe (same as in panels A and B), and subsequently to an actin-specific probe to check that approximately equal amounts of polyA$^+$ RNA had been loaded on each lane. Molecular weight was calculated using a standard marker (BRL).
32. We thank S. Schwarz-Sommer for the scanning electron micrograph, P. Huijser for advice with the microscopical work, and S. C. Schulze for technical assistance. Supported by a European Molecular Biology Organization short-term fellowship to J.J.E. and the "Regeneration" European Economic Community project.

8 July 1991; accepted 2 October 1991

Structural Basis for the Activation of Glycogen Phosphorylase b by Adenosine Monophosphate

STEPHEN R. SPRANG,* STEPHEN G. WITHERS, ELIZABETH J. GOLDSMITH, ROBERT J. FLETTERICK, NEIL B. MADSEN

The three-dimensional structure of the activated state of glycogen phosphorylase (GP) as induced by adenosine monophosphate (AMP) has been determined from crystals of pyridoxalpyrophosphoryl-GP. The same quaternary changes relative to the inactive conformation as those induced by phosphorylation are induced by AMP, although the two regulatory signals function through different local structural mechanisms. Moreover, previous descriptions of the phosphorylase active state have been extended by demonstrating that, on activation, the amino- and carboxyl-terminal domains of GP rotate apart by 5°, thereby increasing access of substrates to the catalytic site. The structure also reveals previously unobserved interactions with the nucleotide that accounts for the specificity of the nucleotide binding site for AMP in preference to inosine monophosphate.

THE BURST OF CATABOLIC ACTIVITY that fuels rapid and continuous skeletal muscle contraction is sustained by glycogen phosphorylase (GP). Phosphorylase can be independently and coordinately activated by phosphorylation at Ser^{14} in response to hormonal and neuronal signals and by binding AMP (*1*). Phosphorylase occurs in vivo and in vitro as a stable dimer of 97.4-kD subunits related by a twofold axis of symmetry (*2*). On activation, dimers assemble into tetramers (*1*) in which the catalytic sites are occluded by dimer-dimer interactions (*3*). Glycogen is required to dissociate these tetramers into the fully active GP dimers found in vivo (*4*). The active state is also induced by sulfate ions (*5, 6*) which, at high concentration, mimic the phosphoserine group and bind to the AMP and catalytic sites (*7*).

Phosphorylation of GP (converting phosphorylase b, or GPb, into phosphorylase a, or GPa) is accompanied by a major conformational change in the amino terminus (*8*), which, as revealed by the structure of sulfate-activated GP, induces a rotation of subunits within the functional dimer (*3, 7*) that leads to the formation of activated tetramers. The mechanism by which AMP independently activates the dephosphorylated enzyme has not yet been described, since the only reported structure of the activated AMP complex (*3*) was determined from crystals grown in ammonium sulfate, which mimics the effects of phosphorylation. Consequently, it is not known whether AMP alone can induce the rearrangement of the amino terminus, with which it makes no direct contact, or promote the same quaternary structural changes induced by phosphorylation or sulfate ions. In order to resolve this question, we determined the structure of the pyridoxalpyrophosphoryl analog of phosphorylase b (PLPP-GPb) in a complex with AMP. The β-phosphate of the PLPP coenzyme analog occupies the substrate (orthophosphate) subsite in the catalytic site. In the absence of ligands, PLPP-GPb forms dimers. The equilibrium conformation of this molecule, as measured by its affinity for adenosine 5′-monothiophosphate (dissociation constant K_d = 40 μM), is similar to that of the native dephosphorylated enzyme in the presence of saturating glucose-1-phosphate (K_d = 140 μM). Its conversion to the active tetrameric state requires AMP (*9, 10*).

The structure of the tetrameric complex with AMP has been determined by x-ray crystallography to a resolution of 3.0 Å. Orthorhombic crystals (*11*) of PLPP-GPb were grown by using polyethylene glycol 8000 as a precipitant. These crystals can only be obtained in the presence of AMP and differ from the monoclinic form of GP grown in 1.0 M ammonium sulfate (*7*). A complete set of x-ray diffraction data to 3.0 Å was measured and processed as described (*11*) (Table 1). The structure was determined by molecular replacement, and the atomic model was refined to a crystallographic *R* factor of 0.18 with data between 8.0 and 3.0 Å resolution (*11*) (Table 1).

The four subunits of the PLPP-GPb tetramer are related by noncrystallographic molecular 222 symmetry as reported for activated GPb (*3*). Tetramers are formed by isologous interaction between dimers. The average root-mean-square (rms) deviation between subunits, after superposition of all equivalent Cα atoms, is ~0.6 Å (Table 2). Superpositions in which only the β-sheet core residues (*12*) of the subunits were used yielded an rms deviation of less than 0.32 Å, slightly greater than the estimation of coordinate error (0.3 Å) by the method of Luzatti (*13*). Comparisons among previously determined phosphorylase structures (Ta-

S. R. Sprang, Howard Hughes Medical Institute and Department of Biochemistry, University of Texas Southwestern Medical Center, Dallas, TX 75235–9050.
S. G. Withers, Department of Chemistry, University of British Columbia, Vancouver, BC V6T 1Y6.
E. J. Goldsmith, Department of Biochemistry, University of Texas Southwestern Medical Center, Dallas, TX 75235–9050.
R. J. Fletterick, Department of Biochemistry and Biophysics, University of California, San Francisco, CA 94143.
N. B. Madsen, Department of Biochemistry, University of Alberta, Edmonton, Alberta T6G 2H7.

*To whom correspondence should be addressed.

Table 1. Crystal parameters, crystallographic data, and refinement statistics for PLPP-GPb. The space group is $P2_12_12$. Cell constants are a = 169.9 Å, b = 209.9 Å, and c = 123.4 Å. There are 16 subunits per cell and the protein content is 43%.

Data statistics	
Reflections measured (no.)	522,198
Unique reflections to 3 Å (no.)	88,004
R_{merge}*	0.053
Reflections $I > 3\sigma(I)$ (no.)	77,728
Complete at 3.0 Å (%)	99.2
Refinement statistics	
Atoms (no.)	26,268
R_{cryst} (8-3.0 Å)	0.18
R_{cryst} (∞-3.0 Å)	0.22
Rms deviation from ideal†	
Bond lengths (Å)	0.015
Bond angles (degrees)	3.4

*Merging R is defined as $R_{merge} = \Sigma_h \Sigma_i |I(h) - I_i(h)|/\Sigma_h \Sigma_i I_i(h)$, where $I_i(h)$ and $I(h)$ are the ith and the mean measurement of the intensity of reflection h, respectively. The crystallographic R value is $R_{cryst} = \Sigma_h [|F_o(h) - F_c(h)|/\Sigma_h F_o(h)]$, where $F_o(h)$ and $F_c(h)$ are the observed and calculated structure factor amplitudes, respectively. †Rms, root-mean-square.

ble 2) show that PLPP-GPb is overall more similar to sulfate-activated phosphorylase b than to the inactive conformation. The bound AMP molecules were clearly visible in the electron density (Fig. 1), as were the positions of the β-phosphate group of the PLPP (not shown), although neither was included in the atomic model until the last stage of crystallographic refinement.

Binding of AMP occurs at the "activation locus," a bundle of α helices (*12*) that comprises part of the interface between the dyad-related subunits of the phosphorylase dimer. By inserting between subunits (Fig. 2), AMP mediates the quaternary structural changes described below. The nucleotide binds between helix 2 (residues 48 to 78) of one subunit and the cap loop (residues 41 to 47) of the opposite subunit. The tight-binding mode of the nucleotide (Fig. 3) is similar to that observed in complexes with partially activated GPa (with the inhibitor glucose bound) (*14*) and in crystals of activated GPb grown from sulfate (*3*). In the nonproductive binding mode, as seen in the inactive phosphorylase complexes with AMP (*3, 8*) or with the inhibitor ATP (*14*), the nucleotide is bound less deeply within the binding site and makes no close purine-enzyme contacts.

The PLPP-GPb structure reveals a previously unobserved feature of the nucleotide binding site that may account for the specificity of phosphorylase for AMP in preference to inosine monophosphate (IMP). Residues 315 to 325 form an ordered, irregular hairpin loop that flanks the nucleotide binding site. In all previously studied crystal forms of GP (*3, 8, 14–16*), this loop adopts a different conformation and is partly or completely disordered, possibly as a consequence of its involvement in crystal packing contacts. Nevertheless, the 315 to 325 loop appears to be an important AMP binding determinant. The side chain of Phe^{316} forms an edge-to-edge contact with the purine ring of the nucleotide, and the main-chain carbonyl O atoms of residues 315 and 318 form possible hydrogen bonds to the 6-amino group of the purine ring (Fig. 3). Adenosine monophosphate is a strong activator (*17, 18*) that binds tightly to the active enzyme (K_d = 3 μM), whereas IMP binds and activates poorly (K_d = 1.4 mM) (*17, 19*). The inosine ring, which has a keto group at the 6 position, cannot act as a hydrogen-bond donor at this position as proposed for AMP and thus presumably cannot form a fully productive complex with the enzyme.

Adenosine monophosphate and phosphorylation do not produce identical structural changes within the activation locus (*12*). On phosphorylation of Ser^{14}, the 22 amino-terminal residues undergo a transition from a partially disordered state and rotate 90° about residue 23 (*20*) to fold into a crevice between the dyad-related subunits of the dimer (*3, 8*). The Ser^{14} phosphate forms ion pairs with Arg^{69} of the α2 helix and Arg^{43} in the cap (residues 41 to 47) of the opposite subunit (Fig. 2). In activated GPb (*7*), a sulfate ion bound at the phosphoserine site promotes the same structural change.

In contrast, the amino terminus is only partially ordered in the AMP-activated PLPP-GPb crystals (Fig. 2); no electron density is observed for amino acid residues 1 to 9 and is weak for residues 10 to 19, which fold in a conformation similar to that observed in the phosphorylated and sulfate-bound structures. The side chains of residues 43 and 69 are poorly ordered in all four PLPP-GPb subunits. The inability of AMP to promote a fully ordered amino terminus in GPb, as confirmed by cross-linking experiments (*21*), appears not to be due to differences in the conformation of the activation locus (*12*), as indicated by the data shown in Table 2. It is more likely, as suggested (*3*), that covalent phosphorylation neutralizes positive charges in the cap–helix-2 interface and in the amino terminus itself, allowing these structural elements to interact. Nevertheless, AMP binding does appear to partially stabilize the amino terminus.

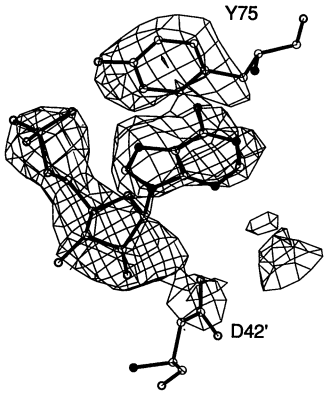

Fig. 1. The volume of the $2F_o - F_c$ electron density map computed at 3.0 Å resolution about the AMP molecule bound to one of the PLPP-GPb subunits and contoured at 1.25 SD above the mean value of the map (*29*). Crystallographic phases were derived from the refined atomic model in which the coordinates of the AMP had not yet been included. Initial coordinates for AMP were derived from Kraut and Jensen (*30*).

Table 2. Comparison of rms deviations after superposition of selected Cα positions of PLPP-GPb subunits with each other and with other phosphorylase subunits. The first row gives the average of all possible superpositions between each of the four PLPP-GPb subunits with the remaining three. The following rows give the mean rms deviation between each of the PLPP-GPb subunits with: row 2, the crystallographically unique subunit of glucose-inhibited GPa (*8*); row 3, the crystallographically unique subunit of inactive GPb (*15*); and row 4, each of the four independent subunits of sulfate-activated GPb (*7*).

Structures compared	Rms deviation		
	Subunit*	Core	Activation locus
PLPP-GPb versus:			
Itself	0.62	0.32	0.31
GPa	1.10	0.60	0.35
Inactive GPb	1.65	0.65	0.52
Activated GPb	1.25	0.51	0.45

*A "subunit" includes residues 20 to 248, 289 to 314, and 325 to 836; residues comprising the core and activation locus are defined in (*12*).

Even though AMP and covalent phosphorylation act at distinct and non-overlapping sites, the two effectors promote similar global conformational changes. Each subunit rotates by 3.5° (relative to glucose-inhibited GPa subunits) about an axis that is nearly perpendicular to the molecular dyad. This axis is positioned near the central interface strand, 185 to 194, which forms a stable fulcrum for the subunit rotation (Fig. 4). The activation loci (*12*), which contain the AMP and phosphorylation sites, are situated on one side of the fulcrum, and the tower helices (residues 265 to 276) that pack together about the dyad axis on the catalytic face of the dimer are located on the other. As the activation loci of the subunits pull together, the tower helices rotate by 60° with respect to each other and reform an alternative packing interface (*3*). Concomitantly, the active site gate (residues 277 to 287), a reverse turn that blocks the catalytic site, becomes disordered, and is not observed in

$2F_o - F_c$ maps computed with phases from the refined model. The extended loop (residues 250 to 265) that connects the amino terminus of the tower helix to the β sheet is also disordered. The tower is thus suspended at the dimer interface, stabilized only by contacts to its symmetry mate and a short stretch of β strand (245 to 249) from the N-domain (*12*).

Tertiary structural changes within GP subunits are apparent when active and inactive conformations of the subunits are compared by superimposition of the N-domain cores (*12*) followed by determination of the transformation needed to best superimpose the C-domain cores (Fig. 5 and Table 3). On activation, the amino- and carboxyl-terminal domains swivel apart by ~5° about an axis that is roughly orthogonal to both the subunit rotation and dyad axes. The rotation is sufficient to increase the separation between Cα atoms of residue 423 (N-domain) and 723 (C domain) by 4 Å on activation. A similar but smaller domain rotation was observed after glucose was exchanged for maltoheptaose and phosphate in GP crystals (*22*).

The activation locus itself rotates with respect to the N-domain core by 3° (Fig. 5 and Table 3). When combined with the intersubunit rotations, this movement allows the cap–helix-2 interface to maintain contacts with its symmetry mate (*3*) while the N-domain core rotates away from the subunit interface (Fig. 4). With the localization of 315 to 325, an ion pair between Asp^{78} and Arg^{323} is formed that may also promote the reorientation of the activation locus. The direction of the activation locus rotation is the same as that of the C-domain (Fig. 5). The two motions appear to be coupled and each may be directly promoted by AMP. The C- and N-domains may also spring apart in response to the loss of restraining interactions with the active site gate at residues 381 to 385 (N-domain) and at 571, 611, and 612 (C domain).

The results obtained from this work, together with the family of GP structures already determined (*3, 7*), demonstrate that activation by AMP binding and by phosphorylation both promote the rotation of subunits within the GP dimer. Second, the PLPP-GPb structure shows that the two effectors activate by different micromechanisms, both of which promote close contacts between the activation loci of opposing subunits. The phosphorylated amino terminus does so by binding along the exterior surface of the cap–helix-2 interface, by forming ion-pair bonds with the phosphoserine, and by forming additional contacts with the helix 4–helix 5 turn (Fig. 2) (*3, 8*). Adenosine monophosphate, in contrast, is bound to and virtually buried within a pocket at the cap–helix-2 interface and makes extensive interactions with helix-8 (residues 289 to 314) and its carboxyl-terminal loop extension. The nucleotide serves to fix the position of these three structural elements with respect to each other in the activated conformation and thereby mediates both the quaternary and intrasubunit domain reorientations. The ami-

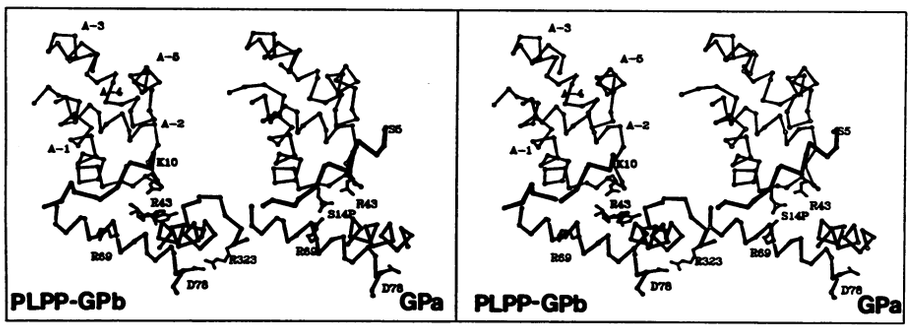

Fig. 2. A Cα trace of the activation locus of PLPP-GPb (left) and glucose-inhibited phosphorylase a (right) viewed along the dyad axis of the functional dimer. One subunit is shown with thick open bonds and the other with thin, filled bonds. The amino termini, residues 5 or 10 to 20 are shown with filled, thick bonds. The side-chain atoms of Arg^{69}, Arg^{43} and Ser^{14} phosphate (GPa), Arg^{323}, and Asp^{78} and for the residues of the loop extending from the carboxyl terminus of helix 8 (PLPP-GPb only) are shown, and AMP is shown at the PLPP-GPb binding site. Structural elements are labeled: A-1, helix 1 (residues 23 to 40); A-2, helix 2 (48 to 78); A-3, helix 3 (94 to 103); A-4, helix 4 (104 to 111); and A-5, helix 5 (118 to 125).

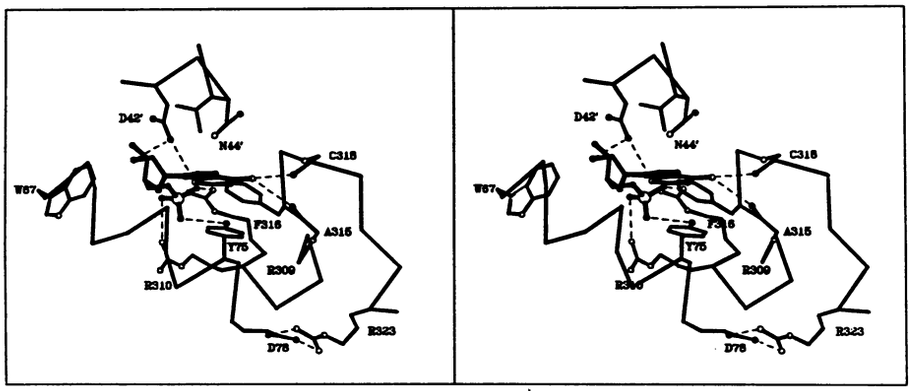

Fig. 3. Detail of the AMP binding site in PLPP-GPb; the view is similar to that shown in Fig. 2. The nucleotide (darkened bonds) adopts the *anti* conformation about the glycosyl bond, the C3′-*endo* ribose conformation, and is *trans* with respect to the C4′-C5′ bond. The phosphate group of AMP is tethered by ion-pair bonds to Arg^{309} and Arg^{310} of helix 8. Asp^{42} is hydrogen bonded to the ribose O2′ hydroxyl group and is within hydrogen-bonding distance of the purine N3. The main-chain carbonyl O atoms of 315 and 318 form hydrogen bonds to the adenine N6 amino group. Phe^{316} is within van der Waals contact distance of the purine ring. AMP forms a parallel stacking interaction with Tyr^{75}. All putative hydrogen bonds involve donor-acceptor heteroatom distances less than 3.3 Å.

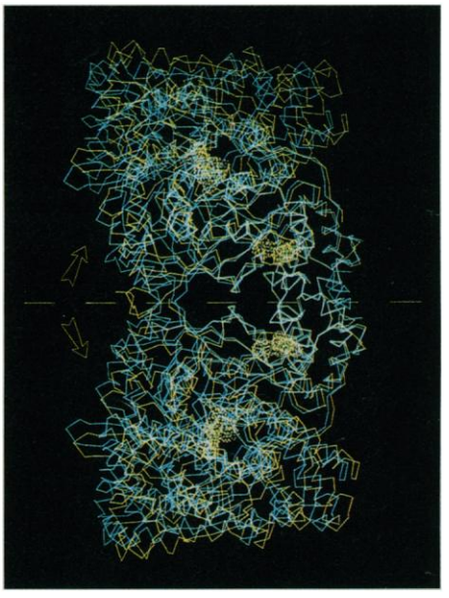

Fig. 4. A dimer of PLPP-GPb (yellow) is shown superimposed upon that of GPa (cyan). The Cα atoms of both activation loci (*10*) (see also legend to Fig. 2) were used to superimpose the dimers. The van der Waals surfaces of the AMP molecules bound to PLPP-GPb sre shown in yellow as are the surfaces of the pyridoxal phosphate coenzymes that mark the catalytic site of GPa. The view is perpendicular to the dyad axis of the functional dimer shown as a dashed orange line. Arrows show the direction of the relative motion of subunits on activation (cyan to yellow) with respect to the dyad axis.

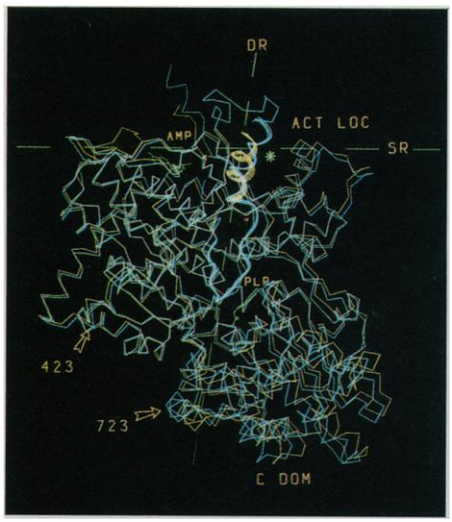

Fig. 5. A subunit of PLPP-GPb (yellow) superimposed on that of glucose-inhibited GPa (cyan). The Cα atoms of the N-domain β-sheet core (*10*) are used to superimpose the subunits. Adenosine monophosphate and pyridoxal phosphate are colored green and labeled. The tower helix (residues 265 to 276) of PLPP-GPb is illustrated as a yellow ribbon, and the tower helix–active site gate (277 to 289) is shown as a cyan ribbon in GPa. The position of the dyad axis of the functional dimer is shown as a green star, the subunit rotation axis is labeled SR, and the axis of relative rotation between the N-domain and C-domain cores is labeled DR. The C-domain (CDOM) and the activation locus (ACT LOC) are labeled. The location of residues 423 and 723 (see text) is shown by arrows.

Table 3. Comparison between PLPP-GPb, the inactive conformation of GPb, and glucose-inhibited GPa with respect to the relative orientation of dyad-related subunits and of subunit domains.

Structural units compared	GPb		gGPa	
	Rot (χ°)*	Rms (Å)	Rot (χ°)	Rms (Å)
Subunit versus subunit	4.6	1.52	3.5	1.06
N-domain versus:				
C-domain	4.5	0.55	4.5	0.48
C-domain core	5.2	0.52	5.2	0.31
Regulatory domain	3.6	0.52	3.0	0.36
Glycogen-binding domain	1.6	0.47	1.4	0.35

*To determine subunit rotation, the activation loci of both subunits of the PLPP-GPb dimer were first superimposed onto corresponding residues of GPb or GPa dimers using Cα atoms; residues 20 to 248 and 289 to 836 of one of the transformed PLPP-GPb subunits were then superimposed onto corresponding atoms of the GPb or GPa subunit. Domain rotations are then calculated by superimposing N-domain core Cα atoms of GPb and GPa onto corresponding atoms of PLPP-GPb followed by determination of the transformation that best superimposes the domains or structural units of interest. The rms deviation shown refers to this transformation. The angle χ describes the transformation as a rotation about a screw axis. The screw axis translation for each of the above transformations was found to be less than 0.2 Å.

no terminus does not become fully ordered on AMP binding. In these respects, the two effectors promote similar global conformational changes by different mechanisms. Activation by AMP binding and by phosphorylation are not mutually exclusive processes and have to some extent additive effects. Even in the presence of saturating AMP, the dephosphorylated enzyme is only 80% as active as GPa (*23*). Similarly, AMP increases the activity of the phosphorylated enzyme by an additional 20% (*24*). The amino terminus, even when dephosphorylated, plays a role in the transmission of conformational changes between subunits, since removal of the 17 amino-terminal residues diminishes the cooperativity of AMP binding while preserving AMP activation (*25*). Thus, the amino terminus may be ordered in the fully activated state.

Third, in addition to the previously reported contacts with the nucleotide, we observe additional interactions that enable the enzyme to distinguish between AMP and IMP. The residues we implicate in this discrimination correspond to the only site within the AMP binding locus in which the primary sequences of the liver and muscle isozymes differ (residues 318 to 323) (*26, 27*). Unlike the muscle isozyme, the liver enzyme is insensitive to AMP activation (*28*). Altered conformational properties of this sequence, together with the loss of the 78-323 ion pair, might account for the inability of AMP to effect an allosteric response in the liver enzyme.

Finally, the PLPP-GPb structure demonstrates, in contrast to previous reports (*3, 7*), that the transition to the activated state is accompanied by a significant rotation of the carboxyl-terminal domain of the subunit relative to the amino-terminal domain. These combined quaternary and tertiary structural changes, by dislodging the active site gate and increasing the separation between the domains that flank the catalytic site, allow GP to engage a bulky oligosaccharide substrate at its catalytic site.

REFERENCES AND NOTES

1. D. J. Graves and J. H. Wang, *Enzymes* **7**, 435 (1972).
2. R. J. Fletterick and N. B. Madsen, *Annu. Rev. Biochem.* **49**, 31 (1980).
3. D. Barford, S.-H. Hu, L. N. Johnson, *J. Mol. Biol.* **218**, 233 (1991).
4. B. Metzger and E. Helmreich, L. Glaser, *Proc. Natl. Acad. Sci. U.S.A.* **57**, 994 (1967).
5. H. D. Engers and N. B. Madsen, *Biochem. Biophys. Res. Commun.* **33**, 49 (1968).
6. D. D. Leonidas *et al.*, *FEBS Lett.* **261**, 23 (1990).
7. D. Barford and L. N. Johnson, *Nature* **340**, 609 (1989).
8. S. R. Sprang *et al.*, *ibid.* **336**, 215 (1988).
9. S. G. Withers, N. B. Madsen, B. D. Sykes, *Biochemistry* **21**, 6716 (1982).
10. ———, *ibid.* **20**, 1748 (1981).
11. PLPP-GPb was prepared as described [S. G. Withers *et al.*, *J. Biol. Chem.* **256**, 10759 (1981)]. Crystals of PLPP-GPb were grown by vapor diffusion from a protein solution (5 to 7 mg/ml) in buffer (50 mM triethanolamine, pH 6.8, 100 mM KCl, 1 mM ethylenediaminetetraacetic acid, 1 mM dithiothreitol) containing 2.5 mM magnesium acetate, 0.5 mM AMP, 12.5 mM maltoheptaose, and 3 to 4% polyethylene glycol 8000 equilibrated against an 8% solution of polyethylene glycol 8000 in buffer at room temperature. Diffraction data were measured at 5°C from five crystals by using a Xuong/Hamlin multiwire detector at the Protein Crystallography Research Resource at UCSD [N.-H. Xuong, C. Nielsen, R. Hamlin, D. Anderson, *J. Appl. Crystallogr.* **18**, 342 (1985)] with graphite-monochromated CuKα x-rays. Data from each crystal were merged separately by using the software of A. J. Howard, C. Nielsen, N.-H. Xuong [*Methods Enzymol.* **114a**, 452 (1985)] and were then merged and scaled together with the program package ROCKS (G. N. Reeke, unpublished results). Examination of the self-rotation function computed with X-PLOR (version 2.1, A. T. Brünger, Yale University, New Haven, CT 1990) with data to 3.0 Å revealed a single peak at $\vartheta = 43°$, $\Phi = 0°$, $K = 180°$. Cross rotation functions were computed with data in the 15 to 3 Å shell by using atomic coordinates of both glucose-inhibited GPa and R-state GPb dimers as search models with vector radii between 5 and 60 Å. After Patterson correlation refinement, in which each subunit was allowed to refine as a rigid unit [A. T. Brünger, *Acta Crystallogr.* **A47**, 195 (1991)], of the highest 200 unique rotation function peaks two solutions (4 × SD above the mean) were found at ($\Theta_1 = 8.5°$, $\Theta_2 = 1.8°$, $\Theta_3 = 159.6°$) and ($\Theta_1 = 288.3°$, $\Theta_2 = 0.9°$, $\Theta_3 = 170.3°$) and were related by the noncrystallographic twofold rotation axis observed in the self-rotation function. Each solution corresponded to one of the two PLPP-GPb dimers in the asymmetric unit. An E(obs)E(calc) correlation translation search [A. T. Brünger, *ibid.*] performed independently for each dimer revealed a single solution at 11 to 12 SD above the mean value of the search function. Least squares rigid-body refinement of the model (a tetramer of glucose-inhibited GPa including all residues except 1 to 20, 248 to 289, 314 to 325, 830 to 841, and AMP) was performed. The electron density map computed from the refined model was inspected by using the graphics program O (version 5.4, T. A. Jones and M. Kjeldgaard, University of Uppsala, Uppsala, Sweden, 1990), which allowed the electron density for all four asymmetric units to be superimposed in the display and an "average" subunit was rebuilt. After a cycle of simulated annealing [A. T. Brünger, J. Kuriyan, M. Karplus, *Science* **235**, 458 (1987)] (2000°C slowly cooling to 300°C) with weighted crystallographic pseudopotentials and noncrystallographic symmetry restraints, and a cycle of Powell minimization (alternating with a manual rebuild of the model where necessary), the crystallographic R value fell to 0.21. Release of noncrystallographic symmetry restraints and restrained refinement of temperature factors reduced the R factor to 0.18. At this stage the AMP and pyridoxalpyrophosphoryl group were included in the model. In the final model, no electron density appears at the glycogen storage or catalytic sites for the maltoheptaose included in the crystallization buffer, nor is electron density observed for residues 1 to 9, 248 to 265, 277 to 288, and 837 to 842.
12. Structural units are defined as follows: N-domain core refers to the β strands that comprise the amino-terminal domain (residues 1 to 482), which, given in N to C strand order are: β17 (residues 190 to 194), β10 (221 to 230), β11 (239 to 244), β4 (153 to 158), β1 (80 to 86), β13 (333 to 338), β14 (371 to 376), β18 (451 to 454), and β19 (479 to 481). C-domain core refers to the β strands that comprise the carboxyl-terminal domain (483 to 836), which given in N to C strand order are: β22 (residues 639 to 646), β21 (599 to 609), β20 (561 to 568), β23 (661 to 668), β24 (686 to 693), and β25 (708 to 714). The structural core of the protein is defined as the N and C domain cores taken together. The activation locus comprises the α-helical elements of the subunit interface on the face of the dimer to which AMP and phosphoserine is bound: α1 (23 to 40), the "cap" (41 to 47), α2 (48 to 78), α3 (94 to

103), α4 (104 to 111), and α5 (118 to 115). Least squares superpositions were performed with a program originally written by W. A. Hendrickson [*Acta Crystallogr.* **A34**, 713 (1986)].
13. P. V. Luzatti, *ibid.* **5**, 802 (1952).
14. S. R. Sprang, E. J. Goldsmith, R. J. Fletterick, *Science* **237**, 1012 (1987).
15. K. R. Acharya, D. I. Stuart, K. M. Varvill, L. N. Johnson, *Glycogen Phosphorylase b: Description of the Protein Structure* (World Scientific, Singapore, 1991).
16. S. R. Sprang and R. J. Fletterick, *J. Mol. Biol.* **131**, 523 (1979).
17. P. L. Mateo, C. Baron, O. Lopez-Mayorga, J. S. Jimenez, M. Cortijo, *J. Biol. Chem.* **259**, 9384 (1984).
18. H. Buc, *Biochem. Biophys. Res. Commun.* **28**, 59 (1967).
19. W. J. Black and J. H. Wang, *J. Biol. Chem.* **243**, 5892 (1968).
20. J. L. Martin, L. N. Johnson, S. G. Withers, *Biochemistry* **29**, 10745 (1990).
21. N. B. Gusev, J. Hajdu, P. Friedrich, *Biochem. Biophys. Res. Commun.* **90**, 70 (1979).
22. E. J. Goldsmith, S. R. Sprang, R. Hamlin, N.-H. Xuong, R. J. Fletterick, *Science* **245**, 528 (1989).
23. H. E. Morgan and A. Parmeggiani, *J. Biol. Chem.* **239**, 2440 (1964).
24. H. D. Engers, S. Shechosky, N. B. Madsen, *Can. J. Biochem.* **48**, 746 (1970).
25. D. J. Graves, S. A. S. Mann, G. Philip, R. J. Oliveira, *J. Biol. Chem.* **243**, 6090 (1968).
26. C. B. Newgard, K. Nakano, P. K. Hwang, R. J. Fletterick, *Proc. Natl. Acad. Sci. U.S.A.* **83**, 8132 (1986).
27. V. L. Rath, C. B. Newgard, S. R. Sprang, E. J. Goldsmith, R. J. Fletterick, *Proteins* **2**, 225 (1987).
28. M. Kobayashi, G. Soman, D. J. Graves, *J. Biol. Chem.* **257**, 14041 (1982).
29. Abbreviations for the amino acid residues are: A, Ala; C, Cys; D, Asp; E, Glu; F, Phe; G, Gly; H, His; I, Ile; K, Lys; L, Leu; M, Met; N, Asn; P, Pro; Q, Gln; R, Arg; S, Ser; T, Thr; V, Val; W, Trp; and Y, Tyr.
30. J. Kraut and L. Jensen, *Acta Crystallogr.* **16**, 79 (1963).
31. We thank L. N. Johnson and D. Barford for making the coordinates of sulfate-activated phosphorylase b available to us (now submitted to the Protein Data Bank as entry 9GPB), to S. Shechosky for excellent technical assistance, to N.-H. Xuong for making the facilities of the Protein Crystallography Research Resource at UCSD available for data collection. Supported in part by NIH research grant. RO1 DK31507 to S.R.S. and RO1 DK26081 to R.J.F. The coordinates of glucose-inhibited phosphosphorylase a and PLPP-GPb have been submitted to the Protein Data Bank.

24 June 1991; accepted 10 September 1991

Characterization of a Zinc Finger Gene Disrupted by the t(15;17) in Acute Promyelocytic Leukemia

AUDREY D. GODDARD, JULIAN BORROW, PAUL S. FREEMONT, ELLEN SOLOMON*

The translocation t(15;17) associated with acute promyelocytic leukemia results in the fusion of the retinoic acid receptor alpha (*RARA*) gene to the *PML* gene. Characterization of *PML* revealed that it is a putative zinc finger protein and potential transcription factor that is commonly expressed, with at least three major transcription products. *PML* breakpoints cluster in two regions on either side of an alternatively spliced exon. Although leukemic cells with translocations characteristically express only one fusion product, both *PML/RARA* (on the 15q+ derivative chromosome) and *RARA/PML* (on the 17q− derivative) are transcribed.

ACUTE PROMYELOCYTIC LEUKEMIA (APL) is characterized cytogenetically by a consistent translocation between chromosomes 15 and 17, t(15;17)(q21;q11.2-12). Both products of the reciprocal translocation are found in these cells (*1*). Investigators have shown that it is the *RARA* gene on chromosome 17 that is disrupted by the translocation (*2, 3*). APL represents an example of a malignancy that is due to a failure of differentiation in which a block in the granulocyte-macrophage pathway leads to the accumulation of abnormal promyelocytes. Treatment of APL promyelocytes with all-trans retinoic acid (RA) in vitro overcomes the block, and this agent has been effective in inducing remission in APL patients (*4*). This observation supports the concept of a role for the RA receptor in the etiology of this disease but leaves open the question of the role of the translocated gene *PML* [formerly *myl* (*3*)] on chromosome 15.

To isolate *PML* cDNA clones, we used a genomic clone (fqp12) (*2*) spanning the t(15;17) breakpoint. With the chromosome 15–specific portion of this clone, we expanded our coverage of the region into 40 kb of genomic DNA (Fig. 1A). Using a genomic fragment (cos15-11/H3.9) as a probe (Fig. 1A), we isolated a total of nine independent overlapping cDNA clones (*5*). Using these cDNAs as probes, we first determined that the normal *PML* locus gives rise to four main transcripts visible on Northern (RNA) blots (Fig. 2). The three largest (4.5, 3.8, and 3.0 kb) are more abundant than the smallest message of 2.1 kb. Northern blots of polyadenylated [poly(A)$^+$] RNA and slot blots of total RNA from a variety of fetal and adult tissues indicated that *PML* was expressed in all tissues examined, including adult brain, gut, liver, lung, muscle, placenta, and testes and fetal brain, gut, liver, and muscle (*6, 7*). The cell lines Daudi (B cell), Molt4 (T cell), HL60 (myeloid), U937 (myeloid) and NB100 (neuroblastoma) were also found to express *PML* (*3, 7*). The four major bands were observed in all RNA samples analyzed on Northern blots. However, some variation in the relative intensity of bands was observed, suggesting some differential regulation is exerted in different tissues.

The nine cDNA clones were sequenced, revealing that three of the four major messages seen on Northern blots were represented in the cDNA clones and that the size differences could be accounted for by alternative 3′-ends. We have designated these *PML-1*, *PML-2*, and *PML-3* (Figs. 1B and 3). The longest of the messages (*PML-1*) is 4463 bp in length and contains a long open-reading frame extending from the initiation codon at position 81 to the first stop codon at position 2261 (*8*). The sequence of the alternative 3′-end (*PML-2*; Fig. 1B) deviates from *PML-1* after codon 548 (they share 1724 bp of cDNA sequence) and represents a transcript 3640 bp in length. The profile of transcripts produced by the *PML* locus is further complicated by the use of alternative splicing. The third class of cDNA clone, *PML-3*, which encodes a 3.0-kb transcript, arises as the result of exclusion of 641 bp from the *PML-2* transcript (base pairs 1725 to 2365) (Fig. 1B) and makes use of an open-reading frame in the *PML-2* 3′-untranslated (UTR) sequences.

The three main classes of transcripts should all encode proteins (Fig. 3) in which the first 548 amino acids are identical. However, 144 bp of alternatively spliced sequence are in this common sequence, and exclusion of this exon from the transcripts results in a loss of 48 amino acids from this part of the putative protein (Figs. 1B and 3A). Beyond residue 548, the three COOH-termini differ. An additional 312 amino acids are encoded in *PML-1*, 41 in *PML-2*, and 254 in *PML-3*. In addition, a third alternatively spliced exon removes 17 amino acids from the *PML-1*–specific COOH-terminal sequences (Fig. 1B).

Whereas the putative *PML* protein sequences do not exhibit a great degree of overall similarity to any known proteins (*9*), the possibility that *PML* protein is involved in transcriptional regulation is suggested by the presence of three clusters of cysteines located towards the NH_2-terminus of all the

A. D. Goddard, J. Borrow, E. Solomon, Somatic Cell Genetics Laboratory, Imperial Cancer Research Fund, London WC2A 3PX, United Kingdom.
P. S. Freemont, Protein Structure Laboratory, Imperial Cancer Research Fund, London WC2A 3PX, United Kingdom.

*To whom correspondence should be addressed.